Spin-dependent transport through two quantum dots embedded in a three-arm ring

2007 J. Phys.: Condens. Matter 19 436212

(http://iopscience.iop.org/0953-8984/19/43/436212)

IOP PUBLISHING JOURNAL OF PHYSICS: CONDENSED MATTER

J. Phys.: Condens. Matter **19** (2007) 436212 (10pp) doi:10.1088/0953-8984/19/43/436212

Spin-dependent transport through two quantum dots embedded in a three-arm ring

Suzhi Wu, Guojun Jin and Yu-qiang Ma

National Laboratory of Solid State Microstructures and Department of Physics, Nanjing University, Nanjing 210093, People's Republic of China

E-mail: gjin@nju.edu.cn

Received 31 May 2007, in final form 1 August 2007
Published 28 September 2007
Online at stacks.iop.org/JPhysCM/19/436212

Abstract

By using the nonequilibrium Green's function technique, we study the coherent electron transport through a three-arm ring with two quantum dots embedded in the upper and lower arm, but without a quantum dot in the middle arm. Gate voltages and magnetic fields are used to tune the linear conductance and the spin polarization at finite temperatures. Four transmission peaks and two conductance dips due to the Fano interference and the on-site Coulomb interactions are observed. The conductance spectra are shown to be sensitive to the magnetic fluxes through the ring, the gate voltages applied in the quantum dots and the Rashba spin–orbit interactions inside the quantum dots. It is found that the spin-polarized conductance is generated by the cooperation of magnetic fluxes and Rashba spin–orbit interactions. Moreover, the spin polarization can be up to 100% when the magnetic fluxes and the Rashba spin–orbit interactions are properly adopted.

1. Introduction

The presence of phase coherence of electrons passing through nanometer structures has attracted remarkable attention during the past several decades. Since the Aharonov–Bohm (AB) effect was realized in a mesoscopic metallic ring [1], there have been many studies on the behavior of the persistent current and energy spectra in single ring [2], double ring [3], Fibonacci ring [4], and multiarm ring structures [5]. On the other hand, due to the confinement of electrons in the three spatial directions, there exist many novel features in transport through a quantum dot (QD), such as the Kondo correlation [6] and the Fano resonance [7, 8]. These novel features have been expected to explore the unknown territory of quantum transport. So far, many physical phenomena, including the AB interference [7–10] and the influence of Coulomb interactions on quantum coherence [11–14], have been investigated.

Recently, devices made of parallel-coupling double QDs [15–18] have been realized experimentally, in which two QDs coupled via barrier tunneling are embedded in opposite arms

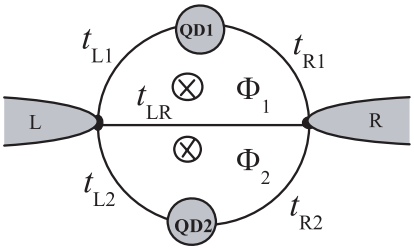

Figure 1. Schematic diagram of a three-arm ring embedded with two QDs, separately, in the upper and lower arms; there is no QD in the middle arm.

of an AB ring connected with the noninteracting leads to external reservoirs. These advances have inspired a number of theoretical attempts to study the transport properties including the resonant tunneling, asymmetric interference patterns, Kondo effect and so on, through two or more QDs arranged in serial configuration [19, 20], parallel configuration [21–25], T-shape configuration [26, 27], or triangular geometry [28] in the absence or presence of strong Coulomb interactions, as well as with or without magnetic fields. Moreover, a substantial amount of dissipationless quantum spin current which could be generated as a result of both actions of electric field and spin–orbit (SO) interaction has been theoretically predicted [29]. Later, Sun *et al* [30] derived a general second quantization form for the SO interaction in the spectral space, which is convenient for handling the SO effect, electron–electron interactions and other interactions for systems with one or more semiconductor QDs.

In this paper, we study the quantum transport through a three-arm ring with one QD embedded in the upper arm and one in the lower arm, but without a QD in the middle arm. There are on-site Coulomb and Rashba SO interactions inside the QDs, and magnetic fluxes through the two half-rings. With the help of the well-established many-body theoretical method, i.e. the Keldysh nonequilibrium Green's function (NEGF) formalism, we examine how the gate voltages and magnetic fields affect the linear conductance and its polarization at finite temperatures. The rest of this paper is organized as follows. In section 2, we describe the model and present the basic formulas of the NEGF used to compute currents. The corresponding numerical results for voltage- and flux-dependent conductances, and related analyses are given in sections 3 and 4. Finally, a summary is presented in section 5.

2. Model and formulation

We consider an open three-arm quantum ring embedded with two QDs and threaded by two different magnetic fluxes in the upper and lower half-rings as shown schematically in figure 1. Two QDs are, respectively, embedded in the upper and lower arms, but there is no QD in the middle arm. Inside the QDs, we consider not only the Coulomb interactions, but also the Rashba SO interactions which affect the transport properties by means of the equivalent Rashba fields in the phase factors. It is assumed that there are no Rashba SO and other interactions in the middle arm.

The total Hamiltonian can be written as

$$\mathcal{H} = \mathcal{H}_{\text{leads}} + \mathcal{H}_{\text{QDs}} + \mathcal{H}_{\text{T}}. \tag{1}$$

In the above equation, $\mathcal{H}_{\text{leads}}$ is the Hamiltonian of the left and right electrodes, and it can be expressed by

$$\mathcal{H}_{\text{leads}} = \sum_{\alpha k\sigma} \varepsilon_{\alpha k} c^{\dagger}_{\alpha k\sigma} c_{\alpha k\sigma}, \tag{2}$$

where $c^{\dagger}_{\alpha k\sigma}(c_{\alpha k\sigma})$ is the creation (annihilation) operator for a conduction electron with spin σ and wavevector k at the α ($\alpha = L, R$) electrode. $\mathcal{H}_{\rm QDs}$ describes the Hamiltonian of the two QDs, each of which has one energy level ε_i and on-site Coulomb interaction with the constant strength U_i,

$$\mathcal{H}_{\rm QDs} = \sum_{i\sigma} \varepsilon_i d^{\dagger}_{i\sigma} d_{i\sigma} + \sum_{i} U_i d^{\dagger}_{i\uparrow} d_{i\uparrow} d^{\dagger}_{i\downarrow} d_{i\downarrow}, \tag{3}$$

where $d^{\dagger}_{i\sigma}$ ($d_{i\sigma}$) is the creation (annihilation) operator of an electron with spin σ in QD i ($i = 1, 2$). The last term $\mathcal{H}_{\rm T}$ in equation (1) includes the contributions from the tunneling effects between the electrodes and the QDs as well as between the electrodes directly through the middle arm,

$$\begin{aligned}\mathcal{H}_{\rm T} = \sum_{ik\sigma}(t_{Li} c^{\dagger}_{Lk\sigma} d_{i\sigma} + {\rm c.c.}) + \sum_{k\sigma}[t_{R1} {\rm e}^{{\rm i}(\phi_1+\phi_2)} {\rm e}^{-{\rm i}\sigma k_R l_1} c^{\dagger}_{Rk\sigma} d_{1\sigma} \\ + t_{R2} {\rm e}^{-{\rm i}(\phi_1+\phi_2)} {\rm e}^{-{\rm i}\sigma k_R l_2} c^{\dagger}_{Rk\sigma} d_{2\sigma} + t_{LR} {\rm e}^{{\rm i}(\phi_1-\phi_2)} c^{\dagger}_{Lk\sigma} c_{Rk\sigma} + {\rm c.c.}],\end{aligned} \tag{4}$$

where $t_{\alpha i}$ is the hopping matrix element between electrode α and QD i, and t_{LR} is the coupling between the electrodes via the middle arm. Since the Rashba SO interactions are taken into account inside the QDs, they are equivalent to a spin-dependent phase factor $-\sigma k_R l_i$ in the hopping matrix elements, where l_i is the size of QD i, and $k_R \equiv m^*\alpha_0/\hbar^2$, with m^* and α_0 being the effective mass of an electron and the interaction coefficient, respectively. Here we notice that the results are completely the same whether the strength of the Rashba SO interaction $k_R l_i$ depends on the position or not. Two magnetic fluxes Φ_1 and Φ_2 are applied in the upper and lower half-rings to change the phase factors, defined by $\phi_1 = 2\pi\Phi_1/\Phi_0$ and $\phi_2 = 2\pi\Phi_2/\Phi_0$, with $\Phi_0 = hc/e$ as the flux quantum. We would emphasize that the Rashba SO interactions $k_R l_1$ and $k_R l_2$ as well as the magnetic fluxes ϕ_1 and ϕ_2 all appear in the phase factors in equation (4), so they will contribute important phase coherence to the system, as will be verified later.

With the Hamiltonian of the system described above, spin-dependent transport properties can be obtained by the standard Keldysh NEGF technique. For our construction, the spin-up or spin-down charge current flowing from the left lead to the center of the structure can be written in the familiar form in the frequency representation [31]

$$I_\sigma = \frac{2e}{\hbar}\int \frac{{\rm d}\varepsilon}{2\pi} {\rm Re}\left[\sum_i t_{Li} G^{<}_{iL\sigma}(\varepsilon) + \tilde{t}_{LR} G^{<}_{RL\sigma}(\varepsilon)\right], \tag{5}$$

where $\tilde{t}_{LR} = t_{LR}{\rm e}^{{\rm i}(\phi_1-\phi_2)}$ and the lesser Green's function (GF) $G^{<}_{XY\sigma}(\varepsilon)$ is the Fourier transform of the time-dependent GF $G^{<}_{XY\sigma}(t) = {\rm i}\langle Y^{\dagger}(0)X(t)\rangle$, $X, Y = c_{\alpha k\sigma}, d_{i\sigma}$. To obtain the current, the main task is to calculate the retarded GF $G^{r}_{XY\sigma}(\varepsilon)$, which is defined by the time-dependent GF as $G^{r}_{XY\sigma}(t) = -{\rm i}\theta(t)\langle\{X(t), Y^{\dagger}(0)\}\rangle$. When the retarded GF is solved, other GFs, such as the advanced GF $G^{a}_{XY\sigma}(\varepsilon)$, whose expression is the Hermitian conjugate of the retarded GF and the lesser GF $G^{<}_{XY\sigma}(\varepsilon)$, can be easily obtained.

In our system, the retarded GF $\boldsymbol{G}^{r}_{\sigma}$ is a 4×4 matrix, and it can be calculated from the Dyson equation

$$\boldsymbol{G}^{r}_{\sigma} = (\boldsymbol{g}^{r-1}_{\sigma} - \boldsymbol{\Sigma}^{r}_{\sigma})^{-1}. \tag{6}$$

Here $\boldsymbol{g}^{r}_{\sigma}$ is the GF of an ideal system without couplings between the electrodes and QDs and between the electrodes through the middle arm, namely, the coupling matrix elements are all assumed zero ($t_{LR} = t_{\alpha i} = 0$). It is obvious that

$$\boldsymbol{g}^{r}_{\sigma}(\varepsilon) = \begin{pmatrix} -{\rm i}\pi\rho_L & 0 & 0 & 0 \\ 0 & -{\rm i}\pi\rho_R & 0 & 0 \\ 0 & 0 & g^{r}_{11\sigma}(\varepsilon) & 0 \\ 0 & 0 & 0 & g^{r}_{22\sigma}(\varepsilon) \end{pmatrix}, \tag{7}$$

where ρ_L (ρ_R) is the density of states of electrode lead L (R) and

$$g^r_{ii\sigma}(\varepsilon) = \frac{\varepsilon - \varepsilon_i - U_i + U_i\langle n_{i\bar{\sigma}}\rangle}{(\varepsilon - \varepsilon_i)(\varepsilon - \varepsilon_i - U_i)}.$$

Here $\langle n_{i\bar{\sigma}}\rangle$ represents the average electron occupation number inside the QDs with the opposite spin $\bar{\sigma}$. In this context, the mean-field treatment is used and the effect of the higher-order self-energy terms on the transport properties is neglected. Thus, one can get the self-energy as

$$\boldsymbol{\Sigma}^r_\sigma(\varepsilon) = \begin{pmatrix} 0 & \tilde{t}_{LR} & t_{L1} & t_{L2} \\ \tilde{t}^*_{LR} & 0 & \tilde{t}_{R1} & \tilde{t}_{R2} \\ t^*_{L1} & \tilde{t}^*_{R1} & 0 & 0 \\ t^*_{L2} & \tilde{t}^*_{R2} & 0 & 0 \end{pmatrix}, \tag{8}$$

where $\tilde{t}_{R1} = t_{R1}\mathrm{e}^{\mathrm{i}(\phi_1+\phi_2)}\mathrm{e}^{-\mathrm{i}\sigma k_R l_1}$, $\tilde{t}_{R2} = t_{R2}\mathrm{e}^{-\mathrm{i}(\phi_1+\phi_2)}\mathrm{e}^{-\mathrm{i}\sigma k_R l_2}$. It is reasonable, in the following analysis, to adopt $t^*_{\alpha i} = t_{\alpha i}$ and $t^*_{LR} = t_{LR}$.

With the result of $\boldsymbol{G}^r_\sigma(\varepsilon)$, the lesser GF $\boldsymbol{G}^<_\sigma(\varepsilon)$ can be straightforwardly obtained from the NEGF equation [14]

$$\boldsymbol{G}^<_\sigma = \boldsymbol{G}^r_\sigma \boldsymbol{g}^{r-1}_\sigma \boldsymbol{g}^<_\sigma \boldsymbol{g}^{a-1}_\sigma \boldsymbol{G}^a_\sigma + \boldsymbol{G}^r_\sigma \boldsymbol{\Sigma}^<_\sigma \boldsymbol{G}^a_\sigma, \tag{9}$$

where $\boldsymbol{g}^<_\sigma(\varepsilon)$ and $\boldsymbol{g}^a_\sigma(\varepsilon)$ are, respectively, the lesser and advanced GFs related to the retarded GF $\boldsymbol{g}^r_\sigma(\varepsilon)$ in the ideal system, while $\boldsymbol{\Sigma}^<_\sigma$ is the lesser self-energy containing all the information of the inelastic processes. Actually, equation (9) includes two contributions on its right-hand side: the elastic part described by the first term and the inelastic one expressed by the second term. In the following treatment, we consider only the coherent transport; the inelastic processes are not important, so we can simply take $\boldsymbol{\Sigma}^<_\sigma = 0$. In addition, $\boldsymbol{g}^{r-1}_\sigma \boldsymbol{g}^<_\sigma \boldsymbol{g}^{a-1}_\sigma$ is diagonal, with $g^{r-1}_{\alpha\alpha\sigma} g^<_{\alpha\alpha\sigma} g^{a-1}_{\alpha\alpha\sigma} = 2\mathrm{i} f_\alpha(\varepsilon)/\pi\rho$ and $g^{r-1}_{ii\sigma} g^<_{ii\sigma} g^{a-1}_{ii\sigma} = 0$, where $f_\alpha(\varepsilon) = 1/[\exp(\varepsilon - \mu_\alpha)/k_\mathrm{B}T + 1]$ is the Fermi–Dirac distribution function in lead α with μ_α as the Fermi energy. As the last step, the intradot electron occupation number $\langle n_{i\bar{\sigma}}\rangle$ needs to be solved self-consistently using the equation

$$\langle n_{i\bar{\sigma}}\rangle = -\mathrm{i}\int_{-\infty}^{+\infty} \frac{\mathrm{d}\varepsilon}{2\pi} G^<_{ii\sigma}(\varepsilon). \tag{10}$$

It is worth pointing out that the mean-field approach to the correlations has a limited range of validity. In the present system, due to the weak couplings between the dots and the leads, the charge fluctuations inside the QDs are small and can be ignored. Therefore, it is reasonable to consider electrons hopping through the dots and interacting with the electrons with opposite spins in the regime of small conductance.

In the next two sections, we apply the formalism of electrical current described above to the differential conductance $\mathcal{G} = \sum_\sigma(\partial I_\sigma/\partial V)$ for a small bias voltage ($V \to 0$). For simplicity, and without loss of generality, in the following numerical calculations we assume the Fermi energies of the source and drain $\mu_L = \mu_R = 1$, and also assume $U_1 = U_2 = 5$, $\rho_L = \rho_R = 1$ and $k_\mathrm{B}T = 10^{-4}$. All the energies are scaled by a certain Fermi energy E_F. The gate voltage V_g will also be denoted as energy by neglecting the multiplying factor of the electronic charge e.

3. Conductance controlled by gate voltages

We first study the effect of the Rashba SO interactions inside the QDs on the linear conductance in the absence of magnetic flux. The energy levels of the QDs are controlled by the gate voltages ($\varepsilon_i = V_{\mathrm{g}i}$). We consider the two dot–lead couplings to be the same, and take $t_{Li} = t_{Ri} = 0.4$ and $t_{LR} = 0.1$. We further assume that the gate voltage of the upper arm QD is larger than that of lower arm QD and set their energy level difference: $V_{\mathrm{g}2} - V_{\mathrm{g}1} = 0.8$. Figure 2 shows

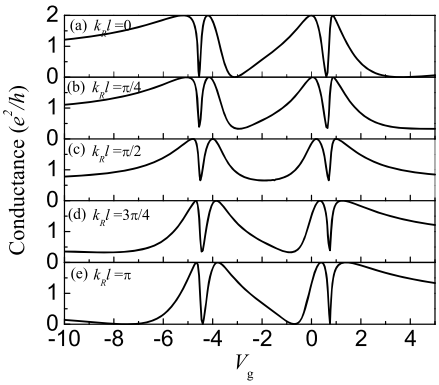

Figure 2. Conductance $\mathcal{G}$ versus gate voltage $V_g = V_{g2} = V_{g1} + 0.8$ for the different strengths of the Rashba SO interactions.

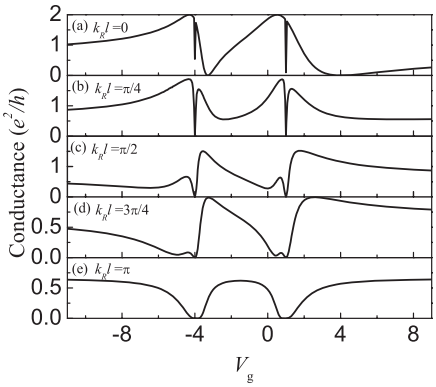

Figure 3. Conductance $\mathcal{G}$ versus gate voltage V_g for $V_{g1} = V_{g2} = V_g$ in the case of $k_Rl_1 = k_Rl_2/2 = k_Rl$ at different values of k_Rl.

the curves of conductance versus the gate voltage for different $k_Rl (k_Rl_1 = k_Rl_2 = k_Rl)$. The curves are dominated by four resonant peaks forming two pairs; each of them is split by a remarkable dip. This result is obviously relevant to the discrete levels at the two QDs and the on-site Coulomb interactions.

In the absence of the Rashba SO interaction ($k_Rl = 0$), there appear the typical Fano resonance peaks resulting from the interference of two discrete states and one continuum [7, 32]. Figure 2 clearly shows that the Rashba SO interactions strongly modify the Fano resonances. The total conductances of the system display antisymmetry for $k_Rl = 0$ and $k_Rl = \pi$. A similar situation occurs for $k_Rl = \pi/4$ and $k_Rl = 3\pi/4$. However, for $k_Rl = \pi/2$, the conductance is symmetric. The origin of this behavior can be ascribed to the coherent electrons flowing through the upper and lower arms and the Rashba SO interactions inducing the phase factors in the tunneling matrix elements in equation (4).

Compared with the above results, the situation becomes even more intriguing when the SO interactions in the two QDs are unequal. We consider the case that the strength of the SO interaction in the lower arm is greater than that in the upper arm, and take $k_Rl_1 = k_Rl_2/2 = k_Rl$. The effect of the SO interactions on the four transmission peaks is strikingly different, as shown in figure 3. Increasing k_Rl, the height of the two peaks on the left of the two dips decreases

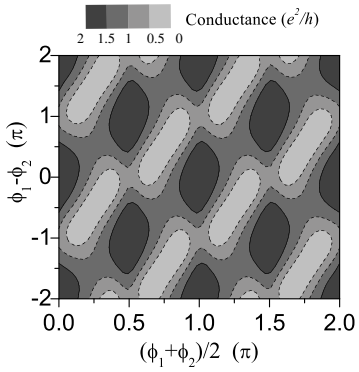

Figure 4. Contours of conductance $\mathcal{G}$ in the $(\phi_1 + \phi_2)/2$ and $\phi_1 - \phi_2$ planes for $V_{g1} = V_{g2} = 0$, $k_R l_1 = k_R l_2 = 0$, $t_{L1} = t_{R1} = 0.35$, and $t_{L2} = t_{R2} = 0.6$.

rapidly; in contrast, the other two peaks on the right of the dips decrease slowly. This is due to the fact that when the strengths of the Rashba SO interactions are varied, the phase shifts are different for the carriers traveling through the upper, middle and lower arms and consequently contribute different interference effects to the total transmission probability. In addition, the linear conductance (in figure 3(e)) shows two valleys at the destructive interference condition ($k_R l = \pi$) around $V_g = -4$ and 1; at the same time, transport is largely suppressed elsewhere.

4. Conductance controlled by magnetic fluxes

Now we turn to study the influence of the two magnetic fluxes ϕ_1 and ϕ_2, applied in the upper and lower half-rings, respectively, on the conductance and polarization. At first, we neglect the effect of the Rashba SO interactions inside the QDs on the transport of the system; that is to say, we assume $k_R l_1 = k_R l_2 = 0$. Figure 4 is a plot of contours of conductance as a function of $(\phi_1 + \phi_2)/2$ and $\phi_1 - \phi_2$ for $V_{g1} = V_{g2} = 0$. From figure 4 one can see that the conductance spectra are strongly affected by both the total and relative values of the two magnetic fluxes, and they oscillate periodically with the magnetic fluxes. The behavior can be validated from the phase factors of the tunneling matrix elements in equation (4).

When the SO interactions inside the QDs are turned on, the current polarization emerges. As usual, the polarization, resulting from the nonequilibrium of electrons with spin up and spin down, is defined as $\eta = (\mathcal{G}_\uparrow - \mathcal{G}_\downarrow)/(\mathcal{G}_\uparrow + \mathcal{G}_\downarrow)$. Figures 5 and 6 are the curves of conductance and their corresponding spin polarization versus the magnetic flux for two configurations, $\phi_1 = -\phi_2 = \phi$ and $\phi_1 = \phi_2 = \phi$. The solid curves in figures 5(a)–(c) and 6(a)–(c) are for $\mathcal{G}_\uparrow$ and the dashed curves are for $\mathcal{G}_\downarrow$. Figures 5(a) and 6(a) show that when $k_R l = 0$, both spin-up and spin-down conductances are the same, so no spin polarization appears (see also the dotted curves in figures 5(d) and 6(d)). In addition, the conductance spectra of these two magnetic configurations present a distinct difference, denoted by the periodic emergence of subpeaks in the latter, due to the influence of the total magnetic fluxes on the phase factors through the ring. In figures 5(b), (c) and 6(b), (c) we find that when $k_R l \neq 0$, a difference appears between the spin-up and spin-down conductances, resulting in generating the spin-polarized conductance (see also figures 5(d) and 6(d)). At the same time, one can easily observe from figures 5 and 6 that the spin-polarized conductance is strongly affected by the strengths of the SO interactions. However, if $\phi_1 = \phi_2 = 0$, $\mathcal{G}_\uparrow$ is equal to $\mathcal{G}_\downarrow$, and the conductance polarization disappears, in spite of the existence of the SO interactions. The reason for this result is explained as

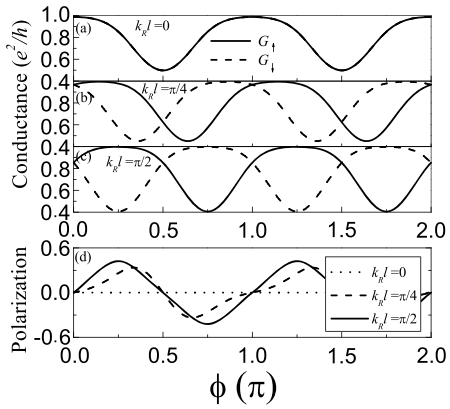

Figure 5. (a)–(c) Conductance $\mathcal{G}$ as a function of magnetic flux for $V_{g1} = V_{g2} = 0$, $t_{L1} = t_{R1} = 0.35$, $t_{L2} = t_{R2} = 0.6$, $\phi_1 = -\phi_2 = \phi$, and different values of Rashba SO interactions $k_R l_1 = k_R l_2 = k_R l = 0, \pi/4, \pi/2$, respectively. (d) Corresponding spin current polarization.

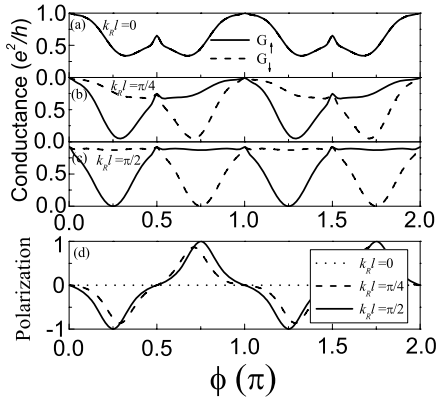

Figure 6. (a)–(c) Conductance $\mathcal{G}$ as the function of magnetic flux for $\phi_1 = \phi_2 = \phi$ and different values of Rashba SO interactions $k_R l_1 = k_R l_2 = k_R l = 0, \pi/4, \pi/2$ respectively. (d) Corresponding spin current polarization. The other parameters are the same as in figure 5.

follows: when $k_R l \neq 0$, the system still has twofold degeneracy for its spin states, which have the same occupation probability, resulting in zero average of spin polarizations. As discussed above, to generate the conductance polarization in our device, a combination of the Rashba SO interactions and magnetic fluxes is necessary.

In order to further explore the effect of the two magnetic fluxes pierced in the upper and lower half-rings on the polarization, in figure 7 we show a plot of the contours of polarization as the function of $(\phi_1+\phi_2)/2$ and $\phi_1-\phi_2$ for $V_{g1} = V_{g2} = 0$, $k_R l_1 = k_R l_2 = \pi/4$. From figure 7, one can clearly discover that the conductance polarization closely depends on the total and relative values of two magnetic fluxes and its values vary from 1 to 0 (dashed–dotted line) and then to -1 when either of the two magnetic fluxes changes. Meanwhile, it is interesting to note that the current always cannot be completely polarized when $(\phi_1 + \phi_2)/2 = n\pi/2$ (n being an integer), whereas it can be fully polarized for any other value of the total magnetic flux. The reason for this fact is interpreted as being that the spin-up (spin-down) electrons reach

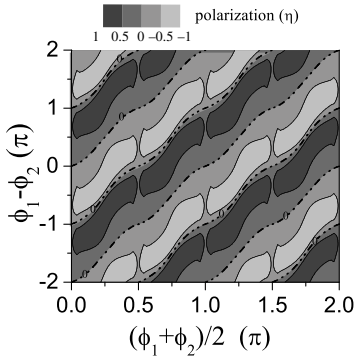

Figure 7. Contours of polarization η in the $(\phi_1 + \phi_2)/2$ and $\phi_1 - \phi_2$ planes for $V_{g1} = V_{g2} = 0$, $k_R l_1 = k_R l_2 = \pi/4$, $t_{L1} = t_{R1} = 0.35$, $t_{L2} = t_{R2} = 0.6$.

destructive interference, and spin-down (spin-up) electrons reach constructive interference under certain conditions, so that $\mathcal{G}_{\uparrow(\downarrow)} = 0$.

From the results obtained above, we can safely come to a conclusion that the conductances and spin polarization of the outgoing currents in this device are predicted to depend on the magnetic fluxes and the Rashba SO interactions. We are interested in the magnitude of the transport current since the complete spin-polarized current can be obtained by tuning the magnetic flux ϕ_i, SO interactions and the gate voltages of the two QDs. For example, in the magnetic flux configuration $\phi_1 = \phi_2 = \phi$, when $V_{gi} = 0$ and $k_R l = \pi/2$, as shown in figure 6(d) (solid line), the polarization η is as large as 100%. It is necessary to point out that, in the present device, the spin polarization of current η is easily controlled by varying the magnetic flux ϕ and gate voltage V_g, both of which can be accessible in experiment, thus allowing the system to manifest the properties of a spin filter.

Here we would like to mention the related works by Tanaka *et al* [24] and Trocha *et al* [25], who studied the system of coupled QDs with ferromagnetic leads, where the two dots are connected via the interdot coupling. In their model, due to the interdot coupling, the conductance spectrum is composed of a broad peak (if the intradot Coulomb interaction $U \neq 0$, the broad peak is split into two) centered at the anti-bonding state and a narrow peak centered at the bonding state with the characteristic Fano line shape. As a comparison, in our model, the Fano resonance is split into four peaks resulting from the upper and the lower QDs' discrete levels as well as the intradot Coulomb interactions. Also, the generations of the spin-dependent currents for both models are under different mechanisms: in the former, the spin-polarized leads give rise to the difference in the densities of states between the spin-up and spin-down conduction electrons, whereas in the latter, spin polarization arises from the combination of the Rashba SO interactions inside the QDs and the magnetic fluxes through the half-rings. As a result, the spin-dependent current is strongly modified by the Rashba SO interactions in the latter, whereas it depends on the polarized strengths of the two leads in the former.

Finally, we would like to give a brief discussion of the possible realization of our system. In this device, the proposed QDs are the gated ones and the are embedded in the upper and lower arms of a AB ring which is penetrated by magnetic fluxes. The leads are coupled to the QDs and to each other via a set of tunnel barriers whose coupled strength can be tuned. It is instructive to estimate the experimentally relevant parameters, especially the Rashba SO parameter. In fact, the Rashba parameter can be controlled electrically. For some regular semiconductors, the Rashba SO interaction strength α_0 can reach 3×10^{-11} eV m, so $k_R = m^* \alpha_0/\hbar^2 \approx 0.015\ \mathrm{nm}^{-1}$

for $m^* = 0.036m_e$. If we take the typical length of a QD $l = 100$ nm, then $k_R l \approx 1.5$. Thus $k_R l$ can reach a value $\sim\frac{\pi}{2}$ or even larger experimentally.

5. Summary

To sum up, we have investigated the spin transport in the system of a three-arm ring with two QDs embedded in the upper and lower arms connected with electrodes based on the well-known NEGF technique. Self-consistent numerical calculations have given us many interesting results. Firstly, there are four conductance peaks due to the on-site Coulomb interactions and the two QDs' discrete levels. Secondly, the Fano line shape is strongly modified by the Rashba SO interaction $k_R l$. Thirdly, when there are no SO interactions inside the QDs, a sub-conductance peak periodically emerges in the parallel magnetic configuration, whereas it does not appear in the antiparallel configuration. Finally, when electrons move through the upper and the lower arms, the Rashba SO interaction inside the QD induces a phase factor in the tunneling matrix elements. By combination of the Rashba SO interactions and the magnetic fluxes, a remarkable spin-dependent current appears. Meanwhile, the spin polarization of the outgoing currents in this device are predicted to be depend on the external magnetic fluxes and Rashba SO interactions. Consequently, tuning of one of these parameters allows the efficient control of the direction and the strength of the spin polarization. Thus, this spintronic device is able to demonstrate the properties of a spin filter.

Acknowledgments

This work was supported by the National Natural Science Foundation of China (Grant Nos 60371013, 10674058, 90601001) and the State Key Program of China (Grant No 2006CB921803).

References

[1] Webb R A, Washburn S, Umbach C P and Laibowitz R B 1985 *Phys. Rev. Lett.* **54** 2696
[2] Büttiker M B, Imry Y and Landauer R 1983 *Phys. Lett.* A **86** 365
[3] Takai D and Ohta K 1994 *Phys. Rev.* B **50** 2685
[4] Jin G J, Wang Z D, Hu A and Jiang S S 1997 *Phys. Rev.* B **55** 9302
[5] Wu H C, Guo Y, Chen X Y and Gu B L 2003 *Phys. Rev.* B **68** 125330
[6] Gerland U, Delft J V, Costi T A and Oreg Y 2000 *Phys. Rev. Lett.* **84** 3710
[7] Schuster R, Buks E, Heiblum M, Mahalu D, Umansky V and Shtrikman H 1997 *Nature* **385** 417
[8] Ryu C-M and Cho S Y 1998 *Phys. Rev.* B **58** 3572
[9] van der Wiel W G, Franceschi S De, Fujisawa T, Elzerman J M, Tarucha S and Kouwenhoven L P 2000 *Science* **289** 2105
[10] Yacoby A, Heiblum M, Mahalu D and Shtrikman H 1995 *Phys. Rev. Lett.* **74** 4047
[11] Georges A and Meir Y 1999 *Phys. Rev. Lett.* **82** 3508
[12] Izumida W, Sakai O and Tarucha S 2001 *Phys. Rev. Lett.* **87** 216803
[13] Hofstetter W and Schoeller H 2002 *Phys. Rev. Lett.* **88** 016803
[14] Haug H and Jauho A-P 1998 *Quantum Kinetics in Transport and Optics of Semiconductors* (Berlin: Springer)
[15] Holleitner A W, Decker C R, Qin H, Eberl K and Blick R H 2001 *Phys. Rev. Lett.* **87** 256802
[16] Holleitner A W, Blick R H, Hüttel A K, Eberl K and Kotthaus J P 2002 *Science* **297** 70
[17] Holleitner A W, Blick R H and Eberl K 2003 *Appl. Phys. Lett.* **82** 1887
[18] Chen J C, Chang A M and Meloch M R 2004 *Phys. Rev. Lett.* **92** 176801
[19] Jiang Z, Sun Q and Wang Y 2005 *Phys. Rev.* B **72** 045332
[20] Nisikawa Y and Oguri A 2006 *Phys. Rev.* B **73** 125108
[21] Kubala B and König J 2002 *Phys. Rev.* B **65** 245301
[22] Zeng Z Y, Claro F and Pérez A 2002 *Phys. Rev.* B **65** 085308

[23] Lu H, Lü R and Zhu B 2005 *Preprint* cond-mat/0511101
[24] Tanaka Y and Kawakami N 2005 *Phys. Rev.* B **72** 085304
[25] Trocha P and Barnaś J 2007 *Phys. Status Solidi* b **244** 2553
[26] Boese D, Hofstetter W and Schoeller H 2002 *Phys. Rev.* B **66** 125315
[27] Martins G B, Büsser C A, Al-Hassanieh K A, Anda E V, Moreo A and Dagotto E 2006 *Phys. Rev. Lett.* **96** 066802
[28] Kuzmenko T, Kikoin K and Avishai Y 2006 *Phys. Rev. Lett.* **96** 06601
[29] Murakami S, Nagaosa N and Zhang S-C 2003 *Science* **301** 1348
[30] Sun Q, Wang J and Guo H 2005 *Phys. Rev.* B **71** 165310
[31] Meir Y and Wingreen N S 1992 *Phys. Rev. Lett.* **68** 2512
[32] Fano U 1961 *Phys. Rev.* **124** 1866